signals that regulate diapause in *Caenorhabditis elegans*. Genes Dev. 13, 1438–1452.

Pierce, S.B., Costa, M., Wisotzkey, R., Devadhar, S., Homburger, S.A., Buchman, A.R., Ferguson, K.C., Heller, J., Platt, D.M., Pasquinelli, A.A., Liu, L.X., Doberstein, S.K., Ruvkun, G., 2001. Regulation of DAF-2 receptor signaling by human insulin and ins-1, a member of the unusually large and diverse *C. elegans* insulin gene family. Genes Dev. 15, 672–686.

Robinson, M.J., Cobb, M.H., 1997. Mitogen-activated protein kinase pathways. Curr. Opin. Cell Biol. 9, 180–186.

Saitoh, M., Nishitoh, H., Fujii, M., Takeda, K., Tobiume, K., Sawada, Y., Kawabata, N., Miyazono, F., Ichijo, H., 1998. Mammalian thioredoxin is a direct inhibitor of apoptosis signal-regulating kinase (ASK) 1. EMBO J. 17, 2596–2606.

Sulston, J.E., Brenner, S., 1974. The DNA of *Caenorhabditis elegans*. Genetics 77, 95–104.

Tanaka-Hino, M., Sagasti, A., Hisamoto, N., Kawasaki, M., Nakano, S., Ninomiya-Tsuji, J., Bargmann, C.I., Matsumoto, K., 2002. SEK-1 MAPKK mediates Ca^{2+} signaling to determine neuronal asymmetric development in *Caenorhabditis elegans*. EMBO Rep. 3, 56–62.

Tobiume, K., Matsuzawa, A., Takahashi, T., Nishitoh, H., Morita, K.-I., Takeda, K., Minowa, O., Miyazono, K., Noda, T., Ichijo, H., 2001. ASK1 is required for sustained activations of JNK/p38 MAP kinases and apoptosis. EMBO Rep. 2, 222–228.

Villanueva, A., Lozano, J., Morales, A., Lin, X., Deng, X., Hengartner, M.O., Kolesnick, R.N., 2001. *jkk-1* and *mek-1* regulate body movement coordination and response to heavy metals through *jnk-1* in *Caenorhabditis elegans*. EMBO J. 20, 5114–5128.

Age-related changes of mitochondrial structure and function in *Caenorhabditis elegans*

Kayo Yasuda [a,b], Takamasa Ishii [a], Hitoshi Suda [c], Akira Akatsuka [b],
Philip S. Hartman [e], Sataro Goto [d], Masaki Miyazawa [a], Naoaki Ishii [a,*]

[a] *Department of Molecular Life Science, Tokai University School of Medicine, Isehara, Kanagawa 259-1193, Japan*
[b] *Teaching and Research Support Center, Tokai University School of Medicine, Isehara, Kanagawa 259-1193, Japan*
[c] *School of High-technology for Human Welfare, Tokai University, Nishino 317, Numazu, Shizuoka 410-0395, Japan*
[d] *Department of Biochemistry, Faculty of Pharmaceutical science, Toho University, Miyama, Funabashi, Chiba 274-8510, Japan*
[e] *Biology Department, Texas Christian University, Fort Worth, TX 76129, USA*

Available online 7 August 2006

Abstract

A number of observations have been made to examine the role that mitochrondrial energetics and superoxide anion production play in the aging of wild-type *Caenorhabditis elegans*. Ultrastructural analyses reveal the presence of swollen mitochondria, presumably produced by fusion events. Two key mitochondrial functions – the activity of two electron transport chain complexes and oxygen consumption – decreased as animals aged. Carbonylated proteins, one byproduct of oxidative stress, accumulated in mitochondria much more than in the cytoplasm. This is consistent with the notion that mitochondria are the primary source of endogenous reactive oxygen species. However, the level of mitochondrially generated superoxide anion did not change significantly during aging, suggesting that the accumulation of oxidative damage is not due to excessive production of superoxide anion in geriatric animals. In concert, these data support the notion that the mitochondrial function is an important aging determinant in wild-type *C. elegans*.
© 2006 Elsevier Ireland Ltd. All rights reserved.

Keywords: Aging; *C. elegans*; mitochondria; oxidative stress

1. Introduction

It is known that energy metabolism figures prominently in the aging process (Balaban et al., 2005). In aerobic organisms, mitochondria are intimately responsible for ATP production via the electron transport chain [oxidative phosphorylation (OXPHOS) system]. Mitochondria also produce reactive oxygen species (ROS) such as superoxide anion (O_2^-), hydrogen peroxide (H_2O_2), and hydroxyl radicals ($^\bullet OH$) as byproducts of energy metabolism. Oxygen is converted to O_2^- by electron leakage from complex I and, to even a larger degree, complex III (Turrens et al., 1985; Lenaz, 1998; Finkel and Holbrook, 2000; Raha and Robinson, 2000). Such endogenously generated ROS readily attack a wide variety of cellular entities, resulting in damage that compromises cell integrity and function (Vuillaume,

1987; Collins et al., 1997). Aging and age-related degenerative diseases may be due to oxidative damage that results from an unfavorable balance between oxidative stress and antioxidant defenses, although it is difficult to distinguish causal events from the myriad of their secondary consequences (Beckman and Ames, 1998; Lenaz, 1998; Finkel and Holbrook, 2000; Raha and Robinson, 2000). For example, both carbonylated protein and lipofusucin accumulate with advancing age, but there is little straightforward evidence to suggest that they strongly act to limit life span (Gerstbrein et al., 2005; Yan et al., 1997; Yan and Sohal, 1998). However, accumulation is more rapid in short-lived mutants and slower in long-lived mutants, thus making these molecules excellent biomarkers of aging if nothing else (Hosokawa et al., 1994; Adachi et al., 1998; Yasuda et al., 1999; Gerstbrein et al., 2005).

Using oxygen consumption as a proxy of metabolism, several groups have demonstrated that metabolism in *Caenorhabditis elegans* decreases rapidly with aging (Braeckman et al., 2002a, 2002b; Houthoofd et al., 2002; Suda et al., 2005).

---

* Corresponding author. Tel.: +81 463 93 1121x2650; fax: +81 463 94 8884.
 E-mail address: nishii@is.icc.u-tokai.ac.jp (N. Ishii).

We employed the novel method of Suda and co-workers for the measurement of energy metabolism, because this method is very simple and accurate. Interestingly, the decrease in respiration began soon after maturation, which is long before significant mortality occurred. In this study, we systematically examined age-related changes in mitochondrial structure and function, including energy metabolism and ROS production in aging populations of wild-type *C. elegans*. We document significant changes in mitochondrial structure and functionality with aging, thus supporting the notion that this organelle plays a key role in life span determination.

2. Methods

2.1. General methods

Wild-type *C. elegans* (N2) animals were cultured as previously described (Brenner, 1974). Embryos (eggs) were collected from nematode growth medium (NGM) agar plates using alkaline sodium hypochlorite (Emmons et al., 1979). The released eggs were allowed to hatch by overnight incubation at 20 °C in S basal buffer (100 mM NaCl, 50 mM potassium phosphate (pH 6.0)) (Sulston and Brenner, 1974). The newly hatched larvae (L1-stage larvae) were cultured on NGM agar plates (3-fold Bacto-peptone) seeded with the *Escherichia coli* (*E. coli*) strain NA22. In order to prevent progeny production, 5-fluoro-2'-deoxyuridine (FudR) (Wako Pure Chemical Industries, Ltd., Osaka, Japan) was added to a final concentration of 40 μM after the animals reached adulthood. The life spans of adult hermaphrodites were determined at 20 °C on NGM agar medium plates seeded with the *E. coli* strain OP50 (Honda et al., 1993; Adachi et al., 1998; Ishii et al., 1998). The surviving fractions for 4-, 8-, 12-, and 15-day-old animals were 100, 100, 99.2 and 97.6%, respectively (data not shown). Experiments were performed five times with starting populations of 69–100 animals. Results were consistent among these experiments.

2.2. Electron microscopy

Staged animals were fixed overnight in 2.5% gluteraldehyde/0.05 M phosphate buffer (pH 7.4) at room temperature. The samples were then washed with 0.1 M phosphate buffer (pH 7.4) and post-fixed in 1% OsO_4/0.05 M phosphate buffer (pH 7.4) for 1 h at 4 °C. After fixation, the samples were dehydrated with a graded ethanol series and embedded in Quetol 812 (Nissin EM Co. Ltd., Tokyo, Japan). Thin sections were stained with 2% uranyl acetate and lead solution and examined under a JEOL 1200 EX electron microscope operating at 80 kV.

2.3. Measurement of energy metabolism

Energy metabolism was determined indirectly by assaying the oxygen consumption rate. Oxygen concentrations were measured using 300 μm aluminum jacketed fiber optic probe that acted as a spectrometer-coupled chemical sensor for full spectral analysis of dissolved or gaseous oxygen pressure (FOXY-2000, Ocean Optics, Inc., FL) (Suda et al., 2005). A fluorescence method measured the partial pressure of dissolved or gaseous oxygen. An optical fiber carried the excitation light produced by the blue LED to the thin film (ruthenium complex) coating the probe tip. The probe collected fluorescence generated at the tip and carried it via the optical fiber to a high-sensitivity spectrometer. When oxygen in the gas or liquid sample diffused into the thin film coating, it quenched the fluorescence. The degree of quenching correlated to the level of oxygen pressure. The oxygen consumption rate was measured on groups of 40 animals in a small closed chamber of about 3 μl volume (1 mm height and 2 mm in diameter). Animals were immersed in a 0.5 μl liquid solution whose composition was the same as the animals' culture medium without agar, including *E. coli*. All oxygen measurements were carried out within 30 min at 22 ± 1 °C. Energy metabolic rate per animal (W) was calculated from oxygen consumption rate per animal by using an energy equivalent of 20.1 J/ml oxygen.

2.4. Isolation of mitochondria

A flotation method was used to remove debris and dead animals from living animals (Lewis et al., 1995). In brief, NGM plates were washed and the contents were suspended in ice-cold S basal buffer and mixed with an equal volume of ice-cold 60% sucrose. After centrifugation for 15 s at 3000 rpm, the floating animals were transferred to a fresh tube. They were washed three times with S basal buffer and once with isolation buffer (210 mM mannitol, 70 mM sucrose, 0.1 mM EDTA and 5 mM Tris–HCl, pH 7.4). The animals were homogenized in isolation buffer using a glass-glass homogenizer with the inclusion of glass beads (0.10–0.11 mm). The debris was removed by a differential centrifugation at 600 × g. The supernatant was then centrifuged at 7200 × g and the mitochondria-containing pellet was suspended in TE buffer (50 mM Tris–HCl (pH 7.4), 0.1 mM EDTA). The supernatant was also retained and served as the cytoplasmic fraction.

2.5. Measurement of activities of complex I and complex II of electron transport chain

The activities of NADH-coenzyme Q oxidoreductase (complex I) and succinate-coenzyme Q oxidoreductase (complex II) in mitochondria were measured as previously described (Trounce et al., 1996). Animals were homogenized in isolation buffer (10 mM Hepes (pH 7.4), 0.15 M NaCl). The resulting homogenate was centrifuged at 250 × g for 10 min to remove debris. The supernatant was further centrifuged at 31,000 × g for 20 min. The pellet was suspended in isolation buffer. Complex I activity was assayed by measuring NADH-sensitive NADH-cytochrome *c* reductase activity at 37 °C in 200 μl 0.1 M Tris–SO₄ buffer pH 7.4, containing 0.32 mg cytochrome *c* and 1 mM sodium cyanate. Complex II activity was assayed by measuring malonate-sensitive succinate-cytochrome *c* reductase activity. The reference cuvette contained 20 μl of 20% sodium malonate solution.

2.6. Measurement of carbonylated proteins

Carbonylated proteins were measured using 2,4-dinitrophenyl hydrazine (DNPH) antibodies. Each fraction was treated with DNPH as described by Levine et al. (1990) with some modifications (Nakamura and Goto, 1996; Ishii et al., 2005). Total protein concentrations and protein concentrations of each fraction were determined using a BCA protein assay kit (Pierce, Rockford, IL). For Western analysis, the samples were transferred to nitrocellulose membranes by a Slot blot method using Milliblot-S (Millipore Co., Tokyo, Japan). The carbonylated proteins were detected with affinity purified anti-DNPH antibodies. Immunoreactive proteins were visualized using the enhanced chemiluminescence system (ECL, Amersham Biosciences, Uppsala, Sweden). A Cool Saver densitometer (ATTO Co., Tokyo, Japan) was employed to quantify results.

2.7. Measurement of superoxide anion (O_2^-)

O_2^- production was measured using the chemiluminescent probe MPEC (2-methyl-6-*p*-methoxyphenylethynyl-imidazopyrazinone)(ATTO Co., Tokyo, Japan) (Shimomura et al., 1998; Ishii et al., 2005). MPEC has an advantage of low background rather than MCLA (3,7-dihydro-2-methyl-6-(4-methoxyphenol) imidazol [1,2-a]pyrazin-3-one) that is generally used. Ten microgram of intact mitochondria was added to 1 ml of assay buffer (50 mM HEPES-NaOH, pH 7.4, 2 mM EDTA) containing 0.7 μM MPEC. Solutions were placed into a photon counter with an AB-2200 type Luminescencer-PSN (ATTO Co., Tokyo, Japan) and measured at 37 °C. The rates of O_2^- were expressed as counts per second.

2.8. Measurement of manganese-supeoxide dismutase (Mn-SOD), voltage-dependent anion channel 1 (VDAC) and cytochrome b large subunit of complex II in electron transport (CYT-1)

Total protein was obtained from animals that were homogenized in isolation buffer with a teflon homogenizer. The debris was removed by centrifugation at 600 × g. Protein concentration was determined using a BCA protein assay kit (Pierce, Rockford, IL). Equal amounts of sample were run on 12.5%

polyacrylamide gels, transferred to polyviniliden difluoride membranes (ATTO Co., Tokyo, Japan), and immunoblotted. Anti-Mn SOD and anti-VDAC polyclonal antibodies were employed as the primary antibodies. They were purchased from Stressgen Bioreagents (British Columbia, Canada) and Santa Cruz Biotechnology, Inc. (CA), respectively. Peroxidase-conjugated secondary antibodies were then used. CYT-1 was used as a reference since levels remain constant during aging (Senoo-Matsuda et al., 2003).

3. Result

3.1. Ultrastructural examination of mitochondria in aging C. elegans

The structures of mitochondria in the body wall muscles of 4-, 10-, and 15-day-old animals were observed using transmission electron microscopy (Fig. 1). In the 4-day-old animals, most mitochondria were relatively small while only a few had long and thin morphologies. In the 10-day-old animals, the structure of some mitochondria was enlarged and swollen. The mitochondria in the 15-day-old animals, which still constituted 90% of the initial population, were more conspicuously enlarged and swollen. In order to prevent progeny production, FudR was routinely used, however, experiments using animals grown in the absence of FudR yielded a similar spectrum of morphological changes (data not shown).

3.2. Oxygen consumption

Fig. 2A shows the profile of energy metabolism for our novel method that was applied to the C. elegans system (Suda et al., 2005). We could significantly detect the signal of oxygen consumption even at the extremely low rate of 0.01%/min. Oxygen consumption was measured in adult populations that were 4-, 8- and 12-days old (Fig. 2B). As indicated in Section 2, metabolic energy was a conversion unit that was directly proportional to the amount of oxygen consumed by groups of 40 adults in a small chamber. Consumption dropped by about

60% between 4- and 8-day-old animals, with another drop of ca. 35% between 8- and 12-day-old animals. Interestingly, there was little mortality during this time, as the survival of 12-day-old animals was over 95%.

3.3. Age-dependent changes in activities of complex I and complex II of electron transport chain

The inner membrane of mitochondria contains five multi-subunit complexes that comprise the electron transport system. The enzyme activities of two of these complexes were assayed in staged populations of C. elegans (Fig. 3). These two complexes were of particular interest because they represent the two entry points of electrons into the electron transport chain. Electrons then move further downstream from these two complexes to coenzyme Q (ubiquinone), at which point they are passed to complex III. The activity of complex I was reduced by 60% in 12-day-old animals as compared to the 4-day-old cohort ($P < 0.0001$). The percent survivals of these two staged populations were both greater than 95%. Thus, there was a significant decline in complex I activity even though most animals were still living. The activity of complex II decreased by 33%, which was not statistically significant at a 0.05 level (Fig. 3).

3.4. Carbonylated proteins accumulate in mitochondria and cytoplasm as C. elegans ages

The levels of carbonylated proteins have been shown to increase with age in many organisms, including C. elegans (Sohal et al., 1993, 1995; Stadtman, 1992). Given that carbonylated proteins are generated by oxidative stress, and that most endogenous free radical generation occurs in mitochondria, carbonylated protein concentrations were determined in mitochondria and cytoplasm isolated from 4-, 8-, 12-, and 15-day-old animals (Fig. 4). The carbonyl content was
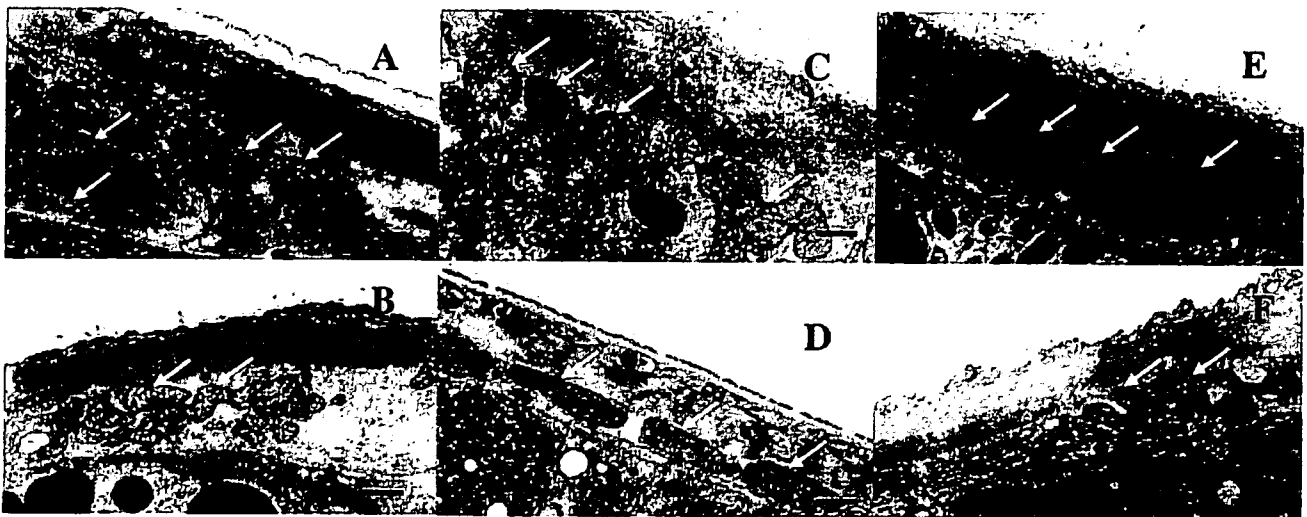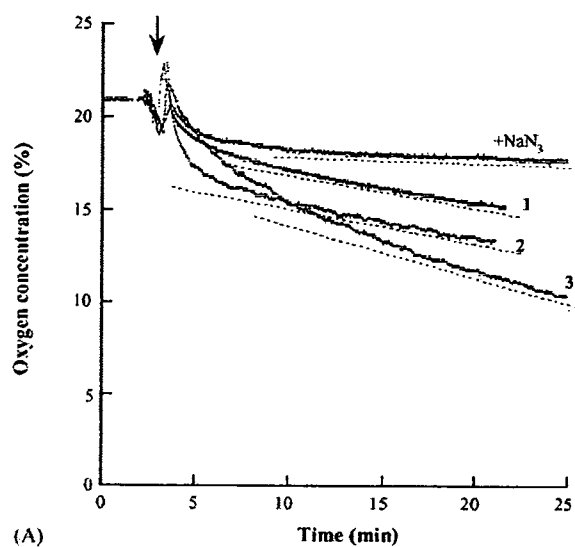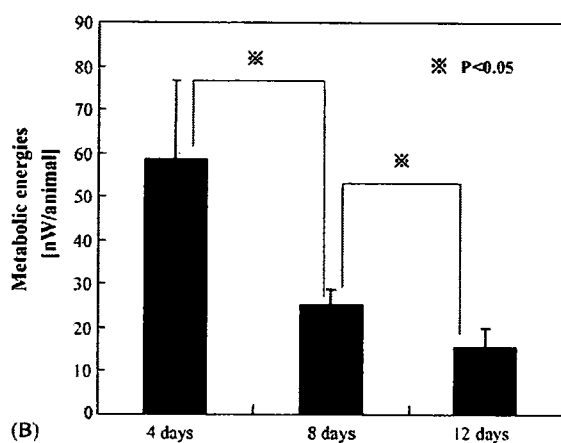

Fig. 1. Age-related changes in the structure of body wall muscle as visualized by transmission electron microscopy. (A), (B) 4-day-old animals; (C), (D) 10-day-old animals; (E), (F) 15-day-old animals. The white arrows indicate mitochondria. Scale bars, 1 μm.

(A)

Time (min)

(B)

Fig. 2. (A) Typical data showing the oxygen consumption of wild-type *C. elegans*. The number of animals transferred from a Petri dish to a small chamber, which were cultured for four days at 20 °C, was 40. Three independent measurements (1, 2, 3) and a control experiment are shown. The control experiment was performed by adding a 0.5-μl solution of sodium azide (NaN₃, 10 mM) into the animal-immersed medium after the measurement of the case 3. Recording of data was started about 10 min after the addition of sodium azide. The oxygen consumption rate per animal and the metabolic energy per animal for three measurements were calculated from the slope of the dashed line, where case-1 was 134 pl/min, 44.8 nW, case-2 was 153 pl/min, 51.2 nW and case-3 was 236 pl/min, 79.1 nW, respectively. Note that every time course was adjusted at the sealing position, which is marked with an arrow. (B) Oxygen consumption as a function of age in wild-type *C. elegans*. The term metabolic energies directly correlate to oxygen consumption. The vertical bars indicate the standard deviation of three separate experiments.

approximately four-fold higher in mitochondria than cytoplasm in young adults (i.e., the 4-day-old cohort). As expected, the mitochondrial concentrations of carbonylated proteins increased in aging animals. The increase was relatively steady and resulted in an approximate doubling of mitochondrial levels over the 11-day span of the experiment. Conversely, cytoplasmic levels remained relatively constant as there was a statistically insignificant increase in cytoplasmic levels between 4 and 8 days, although there was a slight difference between 4 and 12 days ($p < 0.01$). As a result, the ratio of
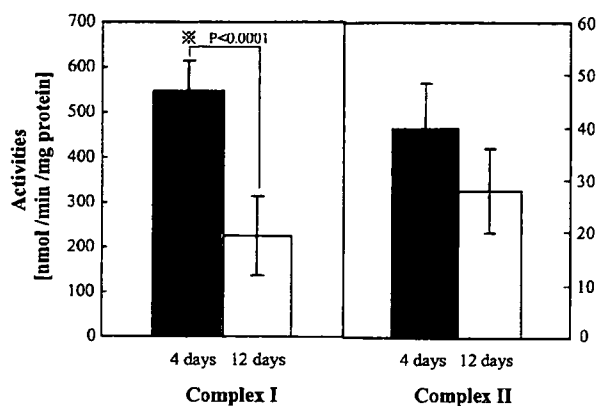

Fig. 3. The activities of complex I and complex II in 4- vs. 12-day-old animals. (A) NADH-cytochrome *c* oxidoreductase as an enzymatic indicator of complex I activity and (B) succinate-coenzyme Q oxidoreductase as an enzymatic indicator of complex II activity. The vertical bars indicate the standard deviation of seven separate experiments.

mitochondrial to cytoplasmic carbonylated proteins increased from ca. 4 to 7.5 between 4 and 11 days of age in wild-type *C. elegans*.

3.5. Amount of O₂⁻ production in mitochondria

Superoxide anions are generated in mitochondria because of the inappropriate single-electron reduction of diatomic oxygen (Raha and Robinson, 2000). To ascertain superoxide anion levels as a function of age, mitochondria were isolated from 4- and 12-day-old animals. O₂⁻ levels were quantified using the chemiluminescent probe MPEC. Superoxide anion levels were slightly lower in mitochondria isolated from the 12-day-old animals, although this difference was not statistically significant (Fig. 5).
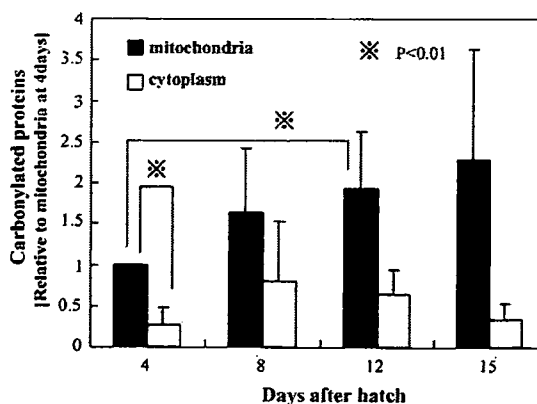

Fig. 4. The relative accumulation of carbonylated protein in the mitochondrial and cytosolic fractions of *C. elegans*. Carbonylated protein content was measured as described in Section 2. All values are relative to that of mitochondrial levels in 4-day-old animals. Comparison of the means by *t*-test reveals significant differences ($p < 0.05$) between the mitochondrial and cytosolic levels at each age. There were statistically differences between 4 days and 12 days in mitochondria ($p < 0.01$), but no difference for 8 days ($p < 0.1$) and for 15 days ($p < 0.2$) as compared with four days, respectively. The vertical bars represent standard deviations from between three to seven separate experiments except two experiments for the cytoplasmic fraction at 15 days.
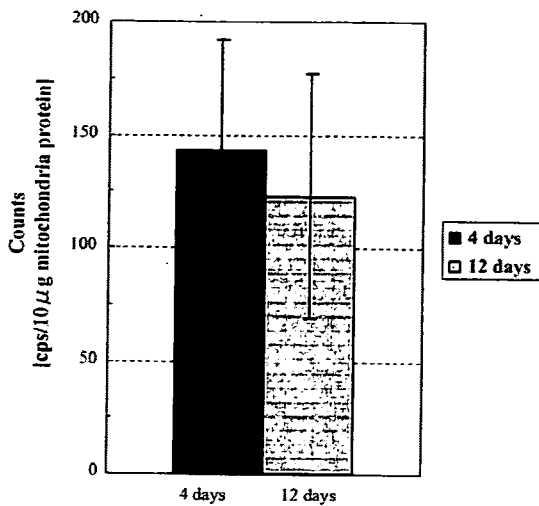
Fig. 5. Superoxide anion production in 4- vs. 12-day-old animals. The error bars indicate the standard deviation of four separate experiments. There was no statistical difference between 4- and 12-day-old animals.

3.6. Mn-SOD, VDAC and CYT-1 levels

It was initially surprising that superoxide anion levels did not increase as animals aged (Fig. 5). To eliminate the possibility that this result might be due to increased levels of the mitochondrial-specific scavenging enzyme Mn-SOD that would counterbalance increased superoxide anion production, we measured Mn-SOD levels using Western blots loaded with whole animals extracts isolated from 4-, 8- and 12-day-old animals (Fig. 6). Although Mn-SOD levels was slightly increased in 8-day-old animal,
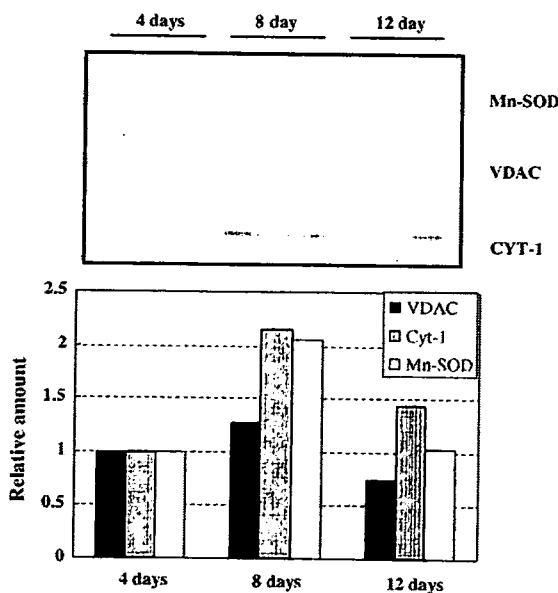

Fig. 6. Age-related changes of mitochondrial protein level. Upper level: an immunochemical assay. Thirty microgram of total protein was applied in each lane. Mn-SOD, VDAC and CYT-1 were detected by described in Section 2. Lower level: quantitative analysis. The detection employed A Cool Saver Densitometer (ATTO Co., Tokyo, Japan).

the levels compared between 4- and 12-day-old animals were unchanged, indicating that the steady state in superoxide anion levels during aging (Fig. 5), reflected reduced production rather than increased removal via enzymatic action in old animals.

CYT-1 is a complex II subunit in mitochondrial inner membrane. VDAC is an integral protein in the mitochondrial outer membrane. Levels of both protein levels held more-or-less constant as animals aged (Fig. 6). In addition, VDAC and CYT-1 protein levels held steady with aging when the input was 150 animals per sample rather than a fixed amount of total protein (data not shown). These results suggest that the decline of mitochondrial function is not caused by a reduction in mitochondrial mass.

4. Discussion

Mitochondria play an indispensable role in the generation of ATP in aerobic eukaryotes. Almost paradoxically, mitochondria are also the primary source of cellular oxidative stress, owing to endogenously generated ROS that result from the combination with free electrons with molecular oxygen. Once generated, ROS can readily attack a wide variety of cellular entities, resulting in cellular, tissue and organ damage that ultimately compromises organismal viability (Beckman and Ames, 1998; Demple and Halbrook, 1983; Vuillaume, 1987; Collins et al., 1997; Balaban et al., 2005). Damage is particularly acute in mitochondria, which presumably results in the progressive deterioration of mitochondrial structure and function. The purpose of the current study was to examine mitochondria and certain of their key reactions as a function of aging in wild-type *C. elegans*.

We first employed transmission electron microscopy to reveal numerous deteriorations in tissue and cellular integrity as wild-type nematodes age (Fig. 1). Herndon et al. (2002) have noted similar changes using both transmission electron and Nomarski DIC microscopy. In particular, we both observed the presence of vacuoles that increase in number and size over time (data not shown). Garigan et al. (2002) employed Nomarski DIC microscopy to this same end.

Given our long-standing interest in mitochondrial structure and function, we were particularly interested in the observation that most mitochondria were relatively small while only a few were long and thin in young adults. In contrast, many mitochondria were enlarged and swollen in 15-day-old animals (Fig. 1). Similar ultrastructural abnormalities have been previously observed in the mitochondria of the precociously aging mutant *mev-1* (Senoo-Matsuda et al., 2003). This also occurs as mice age; specifically, a mitochondrial size increase of 60% was reported in 30-month-old mice as compared to 6-month-old mice (Wilson and Franks, 1975). Quantitative alteration of mitochondria by swelling could lead to ultrastructural pathologies that compromise energy metabolism and the functionality of the various constituent complexes of the electron transport chain.

Mitochondrial swelling could be caused by individual mitochondria increasing in size. Alternatively, mitochondria may undergo fusion events to reduce the number of

mitochondria per cell but increase the size of individual mitochondria. To distinguish these two, the levels of two mitochondrial proteins (CYT-1 and VDAC) per animal were measured in Western blots. The levels of both proteins were unchanged between 4- and 12-day-old animals (Fig. 6), suggesting that overall mitochondrial mass did not change as animals aged. This supports notion that the increased mitochondrial size was the consequence of mitochondrial fusion rather than actual mitochondrial enlargement. In turn, this suggests that the reduction of energy metabolism and complex activities of electron transport chain were due to qualitative rather than quantitative changes in mitochondria.

These ultrastructural changes were accompanied by significant decreases in mitochondrial function. Specifically, oxygen consumption, which we employed as a proxy of respiration, decreased significantly throughout the life span of *C. elegans* (Fig. 2). Similar age-correlated decreases have been noted by the Vanfleteren group (Braeckman et al., 2002a, 2002b; Houthoofd et al., 2002). It is worth noting that a number of different methods have been employed for these determinations (Van Voorhies and Ward, 1999; Braeckman et al., 2002a, 2002b; Suda et al., 2005). There is some controversy as to the reliability of the various experimental approaches (Van Voorhies and Ward, 1999; Braeckman et al., 2002a, 2002b). Nonetheless, the general conclusion that mitochondrial function declines as *C. elegans* ages appears to be on firm footing. This notion is fortified by our observation that the activity of both complexes I and II of the electron transport chain decreased as animals aged (Fig. 3). Interestingly, the decrease in oxygen consumption between 4 and 12 days (ca. 70%), which is presumably a reflection of overall mitochondrial efficiency, was greater than the decreases in two individual components, complex I (ca. 60%) and complex II (ca. 42%), over the same time.

Protein carbonyl derivatives are formed *in vivo* under oxidative stress. Most reports in the literature indicate that protein carbonyls accumulate with aging (Starke-Reed and Oliver, 1989; Sohal et al., 1993, 1995; Beckman and Ames, 1998), including in *C. elegans* (Adachi et al., 1998; Yasuda et al., 1999). In *C. elegans*, they accumulate more rapidly in short-lived mutants and more slowly in long-lived mutants (Adachi et al., 1998; Yasuda et al., 1999) thus making them good "aging markers." While these relationships are informative, we thought it important to determine the intracellular distribution of protein carbonyls. As predicted, we found that the level of carbonylated proteins was significantly higher in mitochondria than in the cytosol of 4-day-old animals (Fig. 4). More interestingly, the level of carbonylated proteins was unchanged in the cytosol but significantly increased in mitochondria as animals aged. Consistent with our present findings, Nagai and co-workers reported age-related increase in mitochondrial protein carbonyls with no significant change in the cytoplasmic proteins (Nagai et al., 2000). This could simply be due to continued accumulation of carbonylated proteins in mitochondria since ROS is mostly produce in mitochondria and therefore produces more damage there than in cytoplasm. Alternatively, it is possible that the export or degradation of mitochondrial carbonylated proteins decreased. Decreased

rates have been reported in the cytoplasmic fraction as rodents age (Goto et al., 2001). The observation that superoxide anion production does not increase with aging (Fig. 5) argues the latter is true. We are aware of one other report in which protein carbonyls were quantified in mitochondria and the cytosol (Davies et al., 2001). Somewhat surprisingly, not only did they report that carbonylaton of proteins did not increase with aging, but levels were equivalent to or even slightly lower in the mitochondria than in the cytosol. We are at a loss to reconcile our results to those of Davies and co-workers.

While not universally the case, age-associated increases in ROS production is reported in the literature (reviewed in Beckman and Ames, 1998). It has been suggested that oxidative damage to the mitochondrial membranes and proteins is the culprit for this effect, with some sort of resultant imbalance in electron transport as the molecular consequence. Counter to our expectations, superoxide anion production did not increase as wild-type animals grew older (Fig. 5). This may be explained as follows. It is generally held that superoxide anion production is dependent upon two primary factors; namely, the membrane potential (or proton motive force) and the degree of coupling reactions as electrons flow through the electron transport system (Hafner et al., 1990; Nicholls, 2002). Specifically, superoxide anion production is favored by a high membrane potential and electron flow that is not tightly coupled. It is possible that these two agents of superoxide anion production have an inverse relationship as *C. elegans* ages; namely, as animals grew older, the relative decline in membrane potential was counterbalanced by the decreased efficiency in coupling reactions between the various complexes. If true, the decline of membrane potential would lead to a decrease in superoxide anion production, while the decline of coupling reaction would lead to an increase. The age-specific decreases in oxygen consumption as well as complexes I and II activities are consistent with notion that membrane potential declines as animals age. While we have no direct evidence that coupling reactions decrease in aging animals, we have previously argued that superoxide anion production is elevated in *mev-1* animals owing to an uncoupling effect of a mutation affecting complex II (Senoo-Matsuda et al., 2001). Alternatively, it is possible that ROS production remained constant, but ROS leakage from mitochondria increased in an age-dependent fashion. Hence, even though the net amount of mitochondrial ROS produced may be the same in young and old worms, the amount leaking from remaining functional complexes varied quite substantially. Such a localized increase in ROS by old mitochondrial ETC complexes may provide an alternate explanation for why protein carbonylation increases with age.

We find it interesting that the age-correlated changes in mitochondrial structure and function manifest themselves long before animals become decrepit and die. For example, oxygen consumption dropped by approximately 56% between four and eight days, with another 39% decrease between 8 and 12 days. Yet survival remained well over 95% over this time span. Others have also noted that structural deterioration proceeds significant mortality (Herndon et al., 2002; Garigan et al.,

2002). This could mean that these various mitochondrial changes are irrelevant to aging, or at the very least secondary consequences of the aging processes. Alternatively, it is possible that they play a causal role in aging, but there is a lag between the onset of cellular- and tissue-level pathologies and the actual time of death. We favor the latter explanation, although it is certainly possible that some of the effects noted are correlative rather than causal. The future challenge is to separate the two.

Acknowledgements

References

Adachi, H., Fujiwara, Y., Ishii, N., 1998. Effects of oxygen on protein carbonyl and aging in Caenorhabditis elegans mutants with long (age-1) and short (mev-1) life spans. J. Gerontol. Biol. Sci. 53A, B240–B244.

Balaban, R.S., Nemoto, S., Finkel, T., 2005. Mitochondria, oxidants, and aging. Cell 120, 483–495.

Beckman, K.B., Ames, B.N., 1998. The free radical theory of aging matures. Physiol. Rev. 78, 547–581.

Braeckman, B.P., Houthoofd, K., De Vreese, A., Vanfleteren, J.R., 2002a. Assaying metabolic activity in ageing Caenorhabditis elegans. Mech. Ageing Dev. 123, 105–119.

Braeckman, B.P., Houthoofd, K., De Vreese, A., Vanfleteren, J.R., 2002b. Assessing metabolic activity in aging Caenorhabditis elegans: Concepts and controversies. Aging Cell 1, 82–88.

Brenner, S., 1974. The genetics of Caenorhabditis elegans. Genetics 7, 71–94.

Collins, A.R., Duthie, S.J., Fillion, L., Gedik, C.M., Vaughan, N., Wood, S.G., 1997. Oxidative DNA damage in human cells: The influence of antioxidants and DNA repair. Biochem. Soc. Trans. 25, 326–331.

Davies, S.M., Poljak, A., Duncan, M.W., Smythe, G.A., Murphy, M.P., 2001. Measurements of protein carbonyls, ortho- and meta-tyrosine and oxidative phosphorylation complex activity in mitochondria from young and old rats. Free Radic. Biol. Med. 31, 181–190.

Demple, B., Halbrook, J., 1983. Inducible repair of oxidative DNA damage in Escherichia coli. Nature 304, 466–468.

Emmons, S.W., Klass, M.R., Hirsh, D., 1979. Analysis of the constancy of DNA sequenced during development and evolution of the nematode Caenorhabditis elegans. Proc. Natl. Acad. Sci. U.S.A. 76, 1333–13337.

Finkel, T., Holbrook, N.J., 2000. Oxidants, oxidative stress and the biology of ageing. Nature 408, 239–247.

Garigan, D., Hsu, A.L., Fraser, A.G., Kamath, R.S., Ahringer, J., Kenyon, C., 2002. Genetic analysis of tissue aging in Caenorhabditis elegans: A role for heat-shock factor and bacterial proliferation. Genetics 161, 1101–1112.

Gerstbrein, B., Stamatas, G., Kollias, N., Driscoll, M., 2005. In vivo spectro-fluorimetry reveals endogenous biomarkers that report healthspan and dietary restriction in Caenorhabditis elegans. Aging Cell 4, 127–137.

Goto, S., Takahashi, R., Kumiyama, A., Radak, Z., Hayashi, T., Takenouchi, M., Abe, R., 2001. Implications of protein degradation in aging. Ann. N.Y. Acad. Sci. 928, 54–64.

Hafner, R.P., Brown, G.C., Brand, M.D., 1990. Analysis of the control of respiration rate, phosphorylation rate, proton leak rate and protonmotive force in isolated mitochondria using the 'top–down' approach of metabolic control theory. Eur. J. Biochem. 188, 313–319.

Herndon, L.A., Schmeissner, P.J., Dudaronek, J.M., Brown, P.A., Listner, K.M., Sakano, Y., Paupard, M.C., Hall, D.H., Driscoll, M., 2002. Stochastic and genetic factors influence tissue-specific decline in ageing C. elegans. Nature 808–814.

Honda, S., Ishii, N., Suzuki, K., Matsuo, M., 1993. Oxygen-dependent perturbation of life span and aging rate in the nematode. J. Gerontol. Bio. Sci. 48, B57–B61.

Hosokawa, H., Ishii, N., Ishida, H., Ichimori, K., Nakazawa, H., Suzuki, K., 1994. Rapid accumulation of fluorescent material with aging in an oxygen-sensitive mutant mev-1 of Caenorhabditis elegans. Mech. Ageing Dev. 74, 161–170.

Houthoofd, K., Braeckman, B.P., Lenaerts, I., Brys, K., De Vreese, A., Eygen, S.V., Vanfleteren, J.R., 2002. Ageing is reversed, and metabolism is reset to young levels in recovering dauer larvae of C. elegans. Exp. Gerontol. 37, 1015–1021.

Ishii, N., Fujii, M., Hartman, P.S., Tsuda, M., Yasuda, K., Senoo-Matsuda, N., Yanase, S., Ayusawa, D., Suzuki, K., 1998. A mutation in succinate dehydrogenase cytochrome b causes oxidative stress and ageing in nematodes. Nature 394, 6694–6697.

Ishii, T., Yasuda, K., Akatsuka, A., Hino, O., Hartman, P.S., Ishii, N., 2005. A mutation in the SDHC gene of complex II increases oxidative stress, resulting in apoptosis and tumorigenesis. Cancer Res. 65, 203–209.

Lenaz, G., 1998. Role of mitochondria in oxidative stress and ageing. Biochim. Biophys. Acta 1366, 53–67.

Levine, R.L., Garland, D., Oliver, C.N., Amici, A., Climent, I., Lenz, A.Z., Ahn, B.W., Shaltiel, S., Stadtman, E.R., 1990. Determination of carbonyl content in oxidatively modified proteins. Methods Enzymol. 186, 464–478.

Lewis, J.A., Fleming, J.T., 1995. Basic culture method. In: Epstein, H.F., Ashakes, D.C. (Eds.), Caenovhabditis elegans: Modern Biological Analysis of an Organism London. Method in Cell Biology. Academic Press U.K., pp. 3–29.

Nagai, M., Takahashi, R., Goto, S., 2000. Dietary restriction initiated late in life can reduce mitochondrial protein carbonyls in rat livers: Western blot studies. Biogerontology 1, 321–328.

Nakamura, A., Goto, S., 1996. Analysis of protein carbonyls with 2,4-dinitrophenyl hydrazine and its antibodies by immunoblot in two-dimensional gel electrophoresis. J. Biochem. 119, 768–774.

Nicholls, D., 2002. Mitchondrial Bioenergetics, Aging, and Aging-related disease. Sci. Aging Knowledge Environ., vol. 31, p. 12 (Review). Science's SAGE KE http://sageke.sciencemag.org/cgi/content/ful/sageke:2002/31/pe12.

Raha, S., Robinson, B.H., 2000. Mitochondria, oxygen free radicals, disease and ageing. Trends Biochem. Sci. 25, 502–508.

Senoo-Matsuda, N., Yasuda, K., Tsuda, M., Ohkubo, T., Yoshimura, S., Nakazawa, H., Hartman, P.S., Ishii, N., 2001. A defect in the cytochrome b large subunit in complex II causes both superoxide anion overproduction and abnormal energy metabolism in Caenorhabditis elegans. J. Biol. Chem. 276, 41553–41558.

Senoo-Matsuda, N., Hartman, P.S., Akatsuka, A., Yoshimura, S., Ishii, N., 2003. A complex II defect affects mitochondrial structure, leading to ced-3- and ca/-4-dependent apoptosis and aging. J. Biol. Chem. 278, 22031–22036.

Shimomura, O., Wu, C., Nurai, A., Nakamura, H., 1998. Evaluation of five imidazopyrazinone-type chemiluminescent superoxide probe and their application to the measurement of superoxide anion generated by Listeria monocytogenes. Anal. Biochem. 258, 230–235.

Sohal, R.S., Agarwal, S., Dubey, A., Orr, W.C., 1993. Protein oxidative damage is associated with life expectancy of houseflies. Proc. Natl. Acad. Sci. U.S.A. 90, 7255–7259.

Sohal, R.S., Agarwal, S., Sohal, B.H., 1995. Oxidative stress and aging in the Mongolian gerbil (Meriones unguiculatus). Mech. Ageing Dev. 81, 15–25.

Stadtman, E.R., 1992. Protein oxidation and aging. Science 257, 1220–1224.

Starke-Reed, P.E., Oliver, C.N., 1989. Protein oxidation and proteolysis during aging and oxidative stress. Arch. Biochem. Biophys. 275, 559–567.

Suda, H., Shouyama, T., Yasuda, K., Ishii, N., 2005. Direct measurement of oxygen consumption rate on the nematode Caenorhabditis elegans by using an optical technique. Biochem. Biophys. Res. Commun. 330, 839–843.

Sulston, J.E., Brenner, S., 1974. The DNA of Caenorhabditis elegans. Genetics 77, 95–104.

Turrens, J.F., Alexandre, A., Lehninger, A.L., 1985. Ubisemiquinone is the electron donor for superoxide formation by complex III of heart mitochondria. Arch. Biochem. Biophys. 237, 408–414.

Trounce, L.A., Kim, Y.L., Jun, A.S., Wallace, D.C., 1996. Assessment of mitochondrial oxidative phosphorylation in patient muscle biopsies, lymphoblasts, and transmitochondrial cell lines. Methods Enzymol. 264, 484–509.

Van Voorhies, W.A., Ward, S., 1999. Genetic and environmental conditions that increase longevity in *Caenorhabditis elegans* decrease metabolic rate. Proc. Natl. Acad. Sci. U.S.A. 96, 11399–11403.

Vuillaume, M., 1987. Reduced oxygen species, mutation, induction and cancer initiation. Mutat. Res. 186, 43–72.

Wilson, P.D., Franks, L.M., 1975. The effect of age on mitochondrial ultrastructure. Gerontologia 21, 81–94.

Yan, L.J., Levine, R.L., Sohal, R.S., 1997. Oxidative damage during aging targets mitochondria aconites. Proc. Natl. Acad. Sci. U.S.A. 94, 11168–11172.

Yan, L.J., Sohal, R.S., 1998. mitochondrial adenine nucleotide translocase is modified oxidatively during aging. Proc. Natl. Acad. Sci. U.S.A. 95, 12896–12901.

Yasuda, K., Adachi, H., Fujiwata, Y., Ishii, N., 1999. Protein carbonyl accumulation in aging dauer formation-defecrive (daf) mutants of *Caenorhabditis elegans*. J. Gerontol. Bio. Sci. 54A, B47–B51.

Original Article

Cell growth of the mouse SDHC mutant cells was suppressed by apoptosis throughout mitochondrial pathway

Masaki Miyazawa[1,*], Takamasa Ishii[1,*], Mika Kirinashizawa[1], Kayo Yasuda[1], Okio Hino[2], Philip S. Hartman[3], Naoaki Ishii[1,**]

[1] *Department of Molecular Life Science, Division of Basic Medical Science and Molecular Medicine, Tokai University School of Medicine, Isehara, Kanagawa, Japan;*
[2] *Department of Pathology (II), Juntendo University School of Medicine, Bunkyo-ku, Tokyo, Japan;*
[3] *Department of Biology, Texas Christian University, Fort Worth, Texas, USA.*

Summary   SDHC E69 cells, which overproduce superoxide anions in their mitochondria, were previously established that had a mutation in the SDHC gene of complex II of the respiratory chain. We now demonstrate that tumors formed by NIH 3T3 and SDHC E69 cells showed significant histological differences. Cytoplasmic cytochrome c release from mitochondria was significantly elevated in SDHC E69 cells and was likely caused by superoxide anion overproduction from mitochondria. In addition, the p53 and Ras signal transduction pathways were activated by oxidative stress and may play a key role in the supernumerary apoptosis in SDHC E69 cells. Our results suggest that the development and growth characteristics of hereditary paragangliomas, which are defective in the same complex of electron transport as mouse SDHC E69 cells, may be caused by apoptosis induction by mitochondrial oxidative stress.

Keywords: Mitochondria, Superoxide anion, Oxidative stress, Apoptosis, Paraganglioma

1. Introduction

Major endogenous reactive oxygen species (ROS) are generated from electron leakage during cellular respiration in mitochondria (*1*). The *mev-1* mutant of the nematode *Caenorhabditis elegans* is mutated in the SDHC subunit of complex II in electron transport system (*2*) and produces excessive superoxide anions (O_2^-) in its mitochondria (*3*). This mutant has proven extremely useful for the study of endogenous oxidative stress and its effects on lifespan, apoptosis and mutagenesis (*4,5*). We have recently constructed a transgenic mouse cell line (SDHC E69 cells) with a mutation that mimics *mev-1* (*6*). As in *C. elegans*, excess O_2^- were generated, which led to supernumerary apoptosis and hypermutability (*6*). Interestingly, the

SDHC E69 cells that escaped from apoptosis were frequently transformed and, when the cells were injected under the epithelium of nude mice, they resulted in the production of tumors two weeks after implantation (*6*). Conversely, after wild-type cells (NIH3T3 cells) were injected, they were on the verge of disappearance but were transformed at high frequency by spontaneous mutations during long passage time or culture time. We show in this report that the NIH3T3 wild-type tumors developed with considerable proliferative abilities over the course of further incubation while the tumor mass of SDHC E69 transformed cells did not significantly enlarge.

It has been reported that mutations in the SDHC or SDHD gene of mitochondrial complex II cause some nonchromaffin and hereditary paragangriomas (PGLs) in humans (*7,8*). Therefore, further analysis of SDHC E69 cells may help clarify the molecular mechanism of the tumorigenesis in neoplasms such as PGLs. It is clear that apoptosis and cell-cycle arrest serve as defensive mechanisms to rid organisms from potentially neoplastic cells. However, the molecular mechanisms by which apoptosis is stimulated by ROS overproduction

*These authors contributed equally to this work.
**Correspondence to:* Dr. Naoaki Ishii, Department of Molecular Life Science, Division of Basic Medical Science and Molecular Medicine, Tokai University School of Medicine, 143 Shimokasuya, Isehara, Kanagawa 259-1193, Japan;
e-mail: nishii@is.icc.u-tokai.ac.jp

from mitochondria are not completely understood. In this report, we explored the mitochondrial and cytosolic responses on apoptosis to ROS overproduction in SDHC E69 mitochondria. Specifically, excess apoptosis in SDHC E69 cells was mediated virtually exclusively through the mitochondrial pathway. In addition, p53 and Ras-MEKK pathways were presumably stimulated in the SDHC E69 cells.

2. Materials and Methods

2.1. Cell culture

The cells were cultivated in DMEM medium (Nissui Company, Tokyo) including 2.5% FBS + 2.5% CS in a 5% CO_2 incubator. Cell division and proliferation were examined after synchronous culture in G0 phase into exhaustion of serum medium and at the contact inhibition state in 100-mm tissue culture dishes. For cell growth, 5×10^4 synchronized cells were cultured in a standard medium of 35-mm tissue culture dishes.

In this manuscript, three-month SDHC E69 cells after the establishment and their wild-type cells (NIH3T3 cells) for 3 month cultured cells as progenitors were used. In brief, the three-month SDHC E69 cells showed the loss of contact inhibition and had many apoptotic molecule-like granules during the first month after establishment (6). During the period of colony formation, some clefts characteristics of programmed cell death were found in the center of some colonies (6). In the SDHC E69 cells, the morphology was changed from the typical solid and elongated fibroblasts to smooth and rounded cells (6). Similar changes were evident, although to a lesser degree in the one-month SDHC E69 cells after establishment (6). In addition, the three-month SDHC E69 cells formed multiple layers (6).

2.2. Antibodies and chemicals

Caspase inhibitors Z-Leu-Glu(OMe)-Thr-Asp-(OMe)-FMK (an inhibitor of caspase 8) and Z-Leu-Glu(OMe)-His-Asp(OMe)-FMK (an inhibitor of caspase 9) were purchased from ICN Pharmaceuticals (Irvine). p53 antibody, phospho-p53 (Ser15) antibody, phospho-p38 MAP kinase (Thr180/Tyr182) antibody, phospho-SAPK/JNK (Thr183/Tyr185) antibody and Bid antibody were purchased from Cell Signaling Technology. p21 (C-19) antibody, Bax (N-20) antibody and MEK kinase-1 (C-22) were purchased from Santa Cruz Biotechnology, Inc (Santa Cruz). Anti-cytochrome c monoclonal antibody was purchased form BD PharMingen (San Jose). Anti-rabbit Ig, horseradish peroxidase linked F(ab')₂ fragment (from donkey) and anti-mouse Ig, horseradish peroxidase linked F(ab')₂ fragment (from sheep) were purchased from Amersham Pharmacia Biotech. The luciferase reporter gene pp53-TA-Luc and pTA-Luc vector used in the p53 reporter assay were purchased from Clontech.

2.3. Transfection and luciferase assay

An AP-1 cis-element dependent transcriptional expression vector (pAP-1-TA-Luc) was constructed using the AP-1 cis-element 5' primer (CTAGCTGAGT CAGTGAGTCACTGACTCACTGACTCATGAGTCA GCTGACTCA) and the AP-1 cis-element 3' primer (G ATCTGAGTCAGCTGACTCATGAGTCAGTGAGTC AGTGACTCACTGACTCAG). These were annealed, and this oligonucleotide was inserted at an *NheI-BglII* site in the pE2F-TA-Luc plasmid vector without the E2F binding site. A pE2F-TA-Luc plasmid vector without the E2F binding site (p-TA-Luc) was used as the negative control vector. Transient transfection of pp53-TA-Luc (0.5 µg), pTA-Luc (0.5 µg) and pCMV-β-galactosidase (0.05 µg) or pAP-1-TA-Luc (0.5 µg), p-TA-Luc (0.5 µg) and pCMV-β-galactosidase (0.05 µg) into NIH3T3 and SDHC E69 cell lines was performed using LipofectAMINE Plus reagent (Invitrogen Inc.). Proteins were prepared for luciferase and β-galactosidase analysis 48 h after transfection by addition of lysis buffer (0.625 mM Tris-PO₄ (pH 7.8), 15% glycerol, 2% CHAPS, 1% Lecichin (L-α-phosphachigilcholine), 1% BSA, 0.1 M EGTA, 1 M MgCl₂, 1 M DTT, 0.1 M p-APMSF). These protein lysates were measured for luciferase and β-galactosidase activities using Luminescencer-PSN (ATTO) or SPECTRA MAX 250 (Molecular Devices) after addition of luciferese buffer (20 mM Tricine-NaOH, 1 mM 4MgCO₂ • Mg(OH) •· 5H₂O (pH 2.3), 2.7 mM MgSO₄ • 7(H₂O) (pH 2.3), 0.1 mM EDTA, 33 mM DTT, 0.27 mM CoA-Li, 0.47 mM luciferin, 0.53 mM ATP)) or β-galactosidase buffer (60 mM Na₂HPO₄ • 12H₂O, 10 mM KCl, 1 mM MgCl₂, 40 mM NaH₂PO₄ • 2H₂O, 1.1 mM ONPG, 47.5 mM 2-mercaptoethanol). Samples were then incubated for 1 h at 37°C. Luciferase relative activity was normalized based on β-galactosidase activity levels and luciferase activity levels of p-TA-Luc, pTA-Luc negative control vector.

2.4. Northern blot analysis

Mouse cDNA's for Northern blot analysis were obtained by RT-PCR method using oligonucleotides for MDM2 (5'-GCC ACC AGA AGA GAA ACC-3' and 5'-GCC TGA GCT GAG TTT TCC-3'), p21-Ras (5'-TTG GAG CAG GTG GTG TTG-3' and 5'-ACA CAT CAG CAC ACA GGG-3'), M-Ras (5'-AGT AGT GGT GGG AGA TGG-3' and 5'-AGT TTG TGA GTG CCG GTG-3'), Raf-1/C-Raf (5'-CAT GAG CAC TGT AGC ACC-3' and 5'-ATC TCC ATG CCA CTT GCC-3'), 18s rRNA (5'-TAC CTG GTT GAT CCT GCC-3' and 5'-TTT CGT CAC TAC CTC CCC-3'), actin (5'-TGG AGA AGA TCT GGC ACC-3' and 5'-ACC CAA GAA GGA AGG CTG-3'), and G3PDH (5'-CAC GGC AAA TTC AAC

GGC-3' and 5'-CTT GGC AGG TTT CTC CAG-3').
3 µg of mRNA which was extracted by Oligotex-dT30
Super (Roche) was subjected to Northern Blot analysis.
Mouse cDNA's were random-prime-labeled using the
High prime kit (Roche) with ^{32}P-dCTP (Amersham
Biosciences) and purified using ProbeQuant G-50 Micro
Columns (Amersham Biosciences). After hybridization
for mouse cDNA's filters were stripped and reprobed
for actin and G3PDH to verify that comparable amounts
of RNA had been loaded in all lanes.

2.5. Western blot analysis

After a particular treatment, cells were washed twice
with phosphate buffered saline and incubated on ice
in lysis buffer containing 10 mM Tris-HCl (pH 8.0),
1 mM EDTA, 100 mM NaCl, 0.1% NP-40, 1 mM
DTT and 0.1 mM p-APMSF for 10 min. This was
followed by brief sonication for Western blot analysis
of p53 or p21. Cell lysates for p21 analysis were then
cleared by centrifugation (400 × g) for 5 min, and the
supernatants were used. In Western blot analysis of Bax
or cytochrome c, both the mitochondrial and cytoplasm
fractions were employed. These cell lysates (containing
10-100 µg of protein) were solubilized by boiling after
the addition of 2 × SDS-PAGE sample buffer (0.125
M Tris-HCl (pH 6.8), 10% 2-mercaptoethanol, 4%
SDS, 10% sucrose and 0.004% bromophenol blue).
For the analysis of p38, p-JNK, Bid or MEKK1, cells
were washed twice with phosphate buffered saline and
incubated in SDS-PAGE sample buffer containing 62.5
mM Tris-HCl (pH 6.8), 2% SDS, 50 mM DTT and 10%
glycerol for 10 min on ice followed by brief sonication.
Cell lysates were then cleared by centrifugation (400
× g) for 5 min and the supernatants were directly
subjected to SDS-PAGE. After electrophoresis, the
proteins were transferred to PVDF (polyvinyliden
difluoride) membrane Clearblot membrane (ATTO)
using a Semi-dry blotting machine AE-6677 (ATTO).
To block nonspecific protein binding, membranes
treated for 8 h at 20-25°C with either 0.1% Tween 20,
5% nonfat dried milk in phosphate buffered saline
for analyses of p53, p21, Bax, cytochrome c, Bid or
MEKK1 or 5% bovine serum albumin, 0.1% Tween 20
in TBS (0.02 M Trizma base, 0.137 M NaCl (pH 7.6))
for analyses of phospho-p53 (Ser15), phospho-p38
MAP kinase (Thr180/Tyr182) or phospho-SAPK/JNK
(Thr183/Tyr185). The membranes were treated with
anti- p53, p21, Bax, cytochrome c, or MEKK1 antibody
in phosphate buffered saline containing 0.1% Tween
20, 5% nonfat dried milk, or phospho-p53 (Ser15)
antibody in TBS containing 0.1% Tween 20, 5% bovine
serum albumin at room temperature for 1 h or with
Bid antibody in phosphate-buffered saline containing
0.1% Tween20, 5% nonfat dried milk, or phospho-p38
MAP kinase (Thr180/Tyr182) or phospho-SAPK/JNK
(Thr183/Tyr185) antibody in TBS containing 0.1%

Tween 20, 5% bovine serum albumin at 4°C for 8 h. The
membranes were then washed with the antibody dilution
buffer for 30 min. They were then treated with the ECL-
plus Western blotting detection system (Amersham
Biosciences) after treatment with anti-rabbit or anti-
mouse antibody (for analysis using Bid). They were
then exposed to Hyperfilm™ ECL chemiluminescence
film (Amersham Biosciences) at room temperature for
2 min. The chemiluminescent signals were visualized
with a CS Analyzer and AE-6962 light capture (ATTO).

3. Results

3.1. Morphology of the SDHC E69 cells on nude mouse

It is known that NIH3T3 cells are transformed at high
frequency by spontaneous mutations during long
passage time or culture time. In fact, the cells, which
did not proliferate within two weeks after the injection
under the epithelium of nude mice (Figure 1A), grew
into huge malignant tumors one month (Figure 1B).
Some of the SDHC E69 cells that escaped from
apoptosis underwent transformation, as evidenced by
the fact that SDHC E69 transformed cells caused tumors
within two weeks when injected under the epithelium of
nude mice (Figure 1C) (*6*). The size of tumors remained
unchanged even after one and a half month (Figure 1D).
As expected of actively proliferating neoplasms, the
tumors derived from the NIH3T3 cells had evidence
of the apocytes and the nuclear divisions with
characteristic dense staining of the cytoplasm (Figure
2A). In addition, the margin between the tumor and
the blood vessel was distinct (Figure 2B). In contrast,
The SDHC E69-derived tumors showed no evidence
of nuclear divisions and showed nuclear aggregation
(Figure 2C). They had assumed the posture of a fibrous
tumor, and the blood vessel and tumor border was not
distinct. Moreover, tumor-associated cells were present
(Figure 2D). Thus, the thickness of the tumor cells layer
was less when derived from SDHC E69 cells (Figure
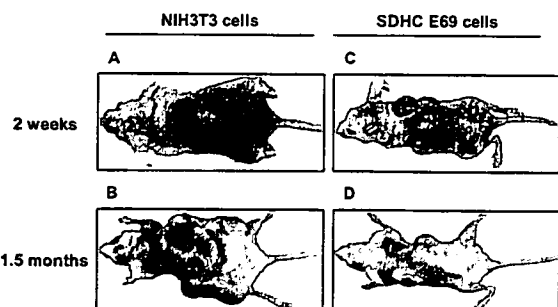2F) versus the wild type cells (Figure 2E).

Figure 1. Comparisons of tumorigenesis using NIH3T3 cells and
SDHC E69 cells injected into the epithelia of nude mice and cultured
for two weeks and one and a half-months. Transplantation of
spontaneous transformation NIH3T3 cells (A and B) and SDHC E69
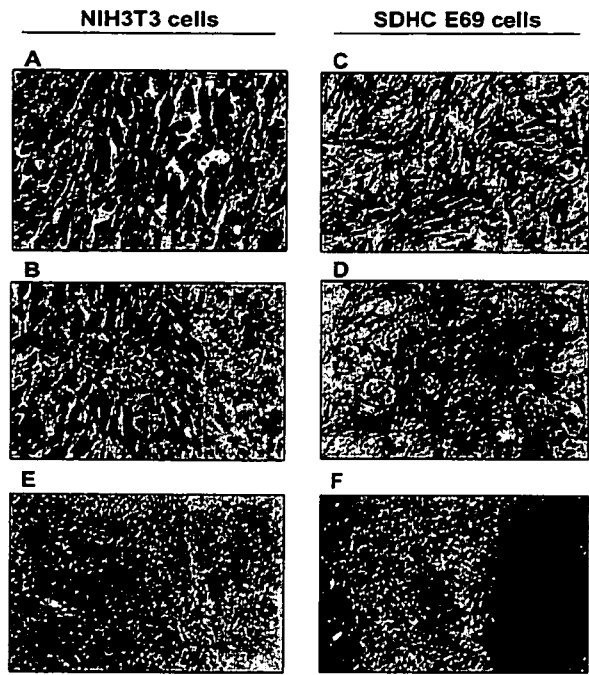cells (C and D) in epithelia of nude mice.

Figure 2. The tissue specimen of the tumor into epithelia of nude mice in spontaneous transformation NIH3T3 cells (A, B, E) and in SDHC E69 cells (C, D, F).

3.2. The role of mitochondrial function to apoptosis

Cellular cytochrome c was found in the mitochondria in both the SDHC E69 cells and NIH3T3 cells (Figure 3A). Cytosolic levels in the SDHC E69 cells and NIH3T3 cells were lower than mitochondrial levels. However, cytosolic cytochrome c levels increased significantly in the SDHC E69 cells.

In the mitochondria of the SDHC E69 cells compared to NIH3T3 cells, the Bax levels were significantly higher (Figure 3A). Bid and tBid levels were barely detectable in the SDHC E69 cells (Figure 3A).

In NIH3T3 cells, MDM2 mRNA expression was equally distributed between the 3.0 kbp and 1.7 kbp mRNAs, which are translated into the p90 and p76 MDM2 proteins, respectively (Figure 3B). A dramatically different pattern was observed in the SDHC E69 cells, as only the short-form type was expressed, which is incapable binding to and promoting p53 protein degradation (Figure 3B). p53 protein levels were below the level of detection in NIH3T3 cells (Figure 3C). Conversely, p53 protein existed in copious
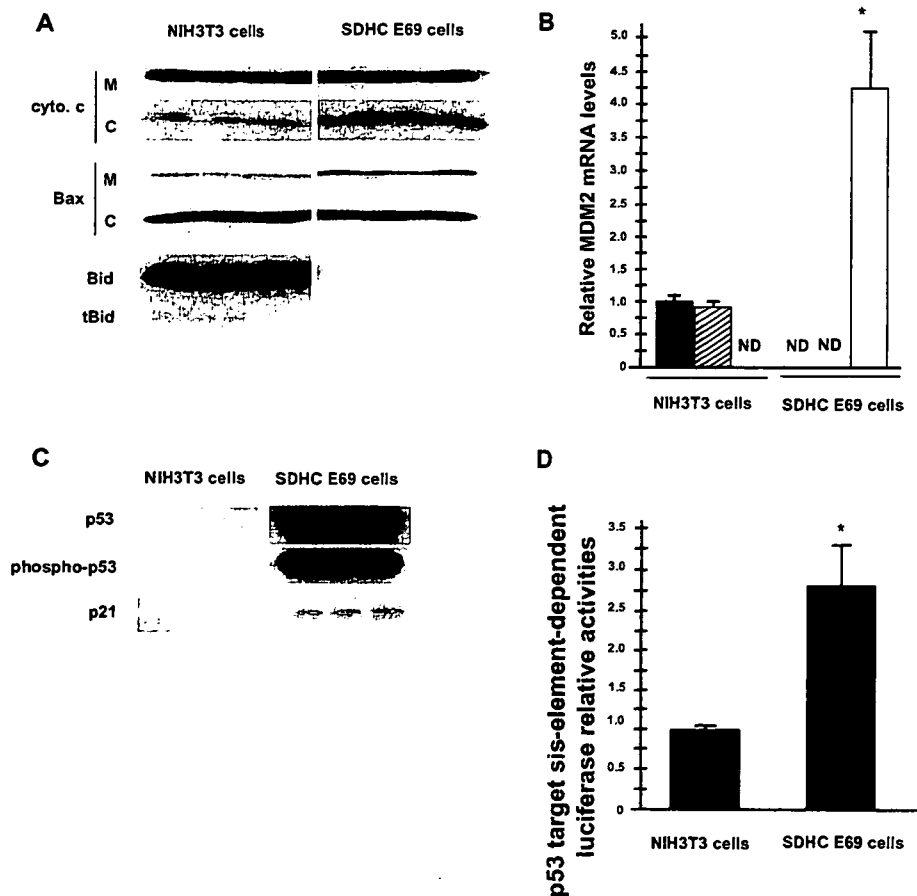

Figure 3. The alteration of cytochrome c release, inducible protein localization and p53 activation in NIH3T3 and SDHC E69 cells. A: Detection of cytochrome c, Bax and Bid proteins levels by Western blot analysis. cyto. c: cytochrome c, M: mitochondrial fraction, C: cytoplasmic fraction. $n = 3$. B: Detection of MDM2 mRNA patterns and expression levels by Northern blot analysis. MDM2 mRNA patterns of 3.0 kbp (p90, full-length MDM2) (closed boxes), 1.7 kbp (p76, not containing p53 binding motif) (hatched boxes) and 1.0 kbp (short form, not containing proteins binding motif) (open boxes) were detected. * $p < 0.01$, $n = 3$. C: Detection of p53, phospho-p53 and p21 protein levels by Western blot analysis. $n = 3$. D: Measurement of p53-dependent transcriptional activation levels by p53 target cis-element-dependent luciferase activity. * $p < 0.01$, $n = 3$.

amounts in the SDHC E69 cells, in which the short-form type MDM2 mRNA was expressed (Figure 3C). Moreover, most of the p53 protein was phosphorylated at serine residue 15 (Figure 3C). In addition, p21 protein was highly expressed in the SDHC E69 cells but not in NIH3T3 cells (Figure 3C). In the each cell lines transiently transfected a luciferase-containing construct with a p53 binding cis-elements, luciferase activity was over 2.8 times higher in the SDHC E69 cells than in the NIH3T3 cells (Figure 3D).

3.3. The role of caspase 8 and caspase 9 on apoptosis

As demonstrated previously, caspase 3 levels were higher in the SDHC E69 cells than in NIH3T3 cells (Figure 4A) (*6*). In the NIH3T3 cells, caspase 3 activity was slightly decreased by each caspase antagonist ($p <$ 0.01) (Figure 4A). Caspase 3 activity was not further reduced by addition of both caspase 8 and 9 antagonists in the NIH3T3 cells (Figure 4A). In the SDHC E69 cells, both caspase 8 and caspase 9 inhibition had a larger effect on caspase 3 activity (Figure 4A). Moreover, we tested the viability of cells cultured in the presence of each caspase antagonist. The survival rate of the NIH3T3 cells was decreased by treatment with a caspase 9 antagonist (Figure 4B).

In contrast to the results obtained with NIH3T3 cells, the presence of each caspase antagonist resulted in increased the cell growth and proliferation in the SDHC E69 cells (Figure 4C). Moreover, both caspase 8 and 9 antagonists were inadequate to substantially reduce caspase 3 activity in the SDHC E69 cells ($p <$ 0.01) (Figure 4A).

3.4. The role of transduction pathway to apoptosis and tumorigenesis

First, we analyzed p21Ras (H-, N-, K-Ras) and M-Ras mRNA expression levels by Northern blot analysis. Relative to the actin and G3PDH internal controls, p21Ras and M-Ras mRNA expression levels in the SDHC E69 cells were increased in comparison with the NIH3T3 cells (Figure 5A).

Relative to the actin and G3PDH internal standards, Raf-1/C-Raf mRNA expression, which induces cell growth and proliferation, was significantly increased in the SDHC cells in comparison to the NIH3T3 cells (Figure 5B). 195 kDa full-length MEKK1 protein was present in unchanged amount in the SDHC E69 cells, but the activated p91kDa MEKK1 protein was increased (Figure 5C). In addition, activated 54 kDa and 46 kDa JNK proteins were present in increased amounts in the SDHC E69 cells (Figure 5C). Conversely, the accumulation of activated p38 MAPK protein was not altered (Figure 5C). An AP-1 cis-element-dependent luciferase assay showed that JNK-dependent transcription was activated in the SDHC E69
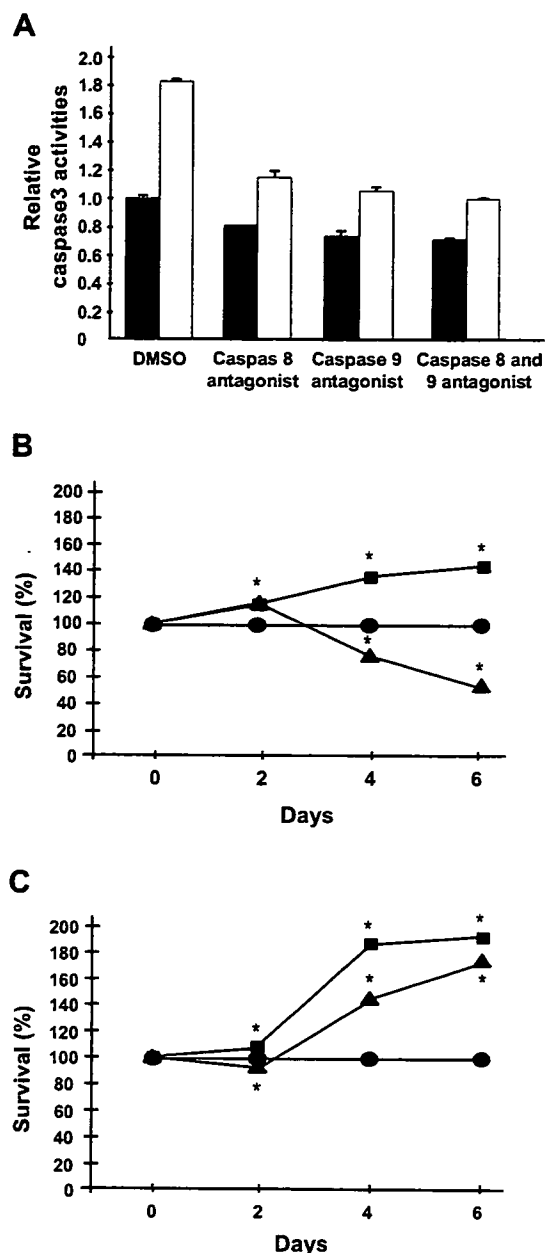

Figure 4. Variation of caspase 3 activity and survival rate by in response to caspase 8 and 9 antagonists. A: Caspase 3 levels were measured in NIH3T3 cells cultured for 3 month (closed boxes) and SDHC E69 cells (open boxes) in the presence of caspase 8 and 9 antogonists. $n = 3$. B and C: Viability of NIH3T3 cells (B), SDHC E69 cells (C) grown in the presence of caspase 8 (■) and caspase 9 (▲) antagonists and DMSO (●) additions. * $p < 0.01$, $n = 3$.

cells (Figure 5D).

4. Discussion

We have previously established a transgenic SDHC E69 mouse cell line that contains a mutated SDHC subunit in complex II of the electron transport system (*6*). The SDHC E69 cells overproduced superoxide anion from mitochondria had elevated cytoplasmic carbonyl proteins and 8-OHdG in their DNA as well
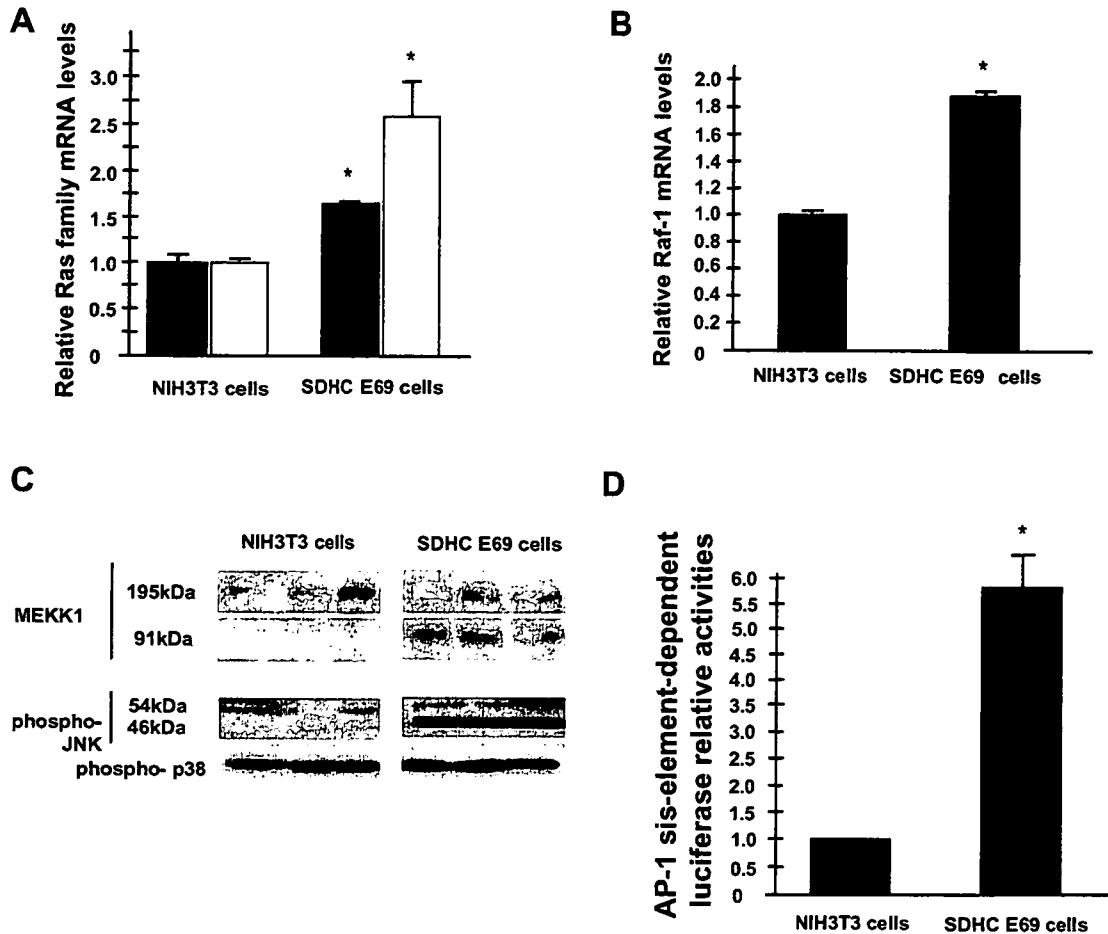
Figure 5. Alteration of stress-induced Ras-Raf and Ras-MEKK signal transduction pathways. A and B: Measurement of p21Ras (H-, N-, K-) (closed boxes), M-Ras (open boxes) (A) and Raf-1 mRNA expression levels (B) by Northern blot analysis. $*p < 0.01$, $n = 3$. C: Detection of MEKK1, phosphorylated JNK and p38 MAPK proteins, which are located and activated in downstream of MEKK1 activation, by Western blot analysis. $n = 3$. D: Measurement of transcriptional activation dependent on JNK activity by AP-1 cis-element-dependent luciferase activity. $*p < 0.01$, $n = 3$.

as significantly higher mutation frequencies than wild type (NIH3T3). There were many apoptotic cells in this cell line, as predicted by the observed increase in caspase 3 activity, decrease in mitochondrial membrane potential and structural changes in their mitochondria (6). In addition, some cells that escaped from apoptosis underwent transformation, as evidenced by the fact that SDHC E69 cells caused tumors within two weeks when injected under the epithelium of nude mice (Figure 1C) (6). The size of tumors remained unchanged even after one month (Figure 1D). It is known that NIH3T3 cells are transformed at high frequency by spontaneous mutations during long passage time or culture time. In fact, the cells, which did not proliferate within two weeks after the injection under the epithelium of nude mice, grew into huge malignant tumors one month (Figure 1A and B).

The SDHC E69-derived tumors showed no evidence of nuclear divisions and showed nuclear aggregation (Figure 2C). They had assumed the posture of a fibrous tumor, and the blood vessel and tumor border was not distinct. Moreover, tumor-associated cells were

present (Figure 2D). In contrast, as expected of actively proliferating neoplasms, the tumors derived from the NIH3T3 cells had evidence of the apocytes and the nuclear divisions with characteristic dense staining of the cytoplasm (Figure 2A). In addition, the margin between the tumor and the blood vessel was distinct (Figure 2B). Thus, the thickness of the tumor cells layer was less when derived from SDHC E69 cells versus the NIH3T3 cells (Figures 2E and F). These histological data are consistent with the notion that the NIH3T3 cells are actively proliferating while the SDHC E69 cells are not. We speculate that there was no increase in overall tumor mass because cell proliferation was counterbalanced by increased levels of apoptosis.

Mitochondria from SDHC E69 cells overproduced O_2^-, leading to wide-spread apoptosis as caspase 3 levels were elevated (6). Caspase 3 acts relatively late in the caspase cascade, after cells are inextricably committed to apoptosis. To elucidate the mechanisms by which overproduction of O_2^- leads to supernumerary apoptosis, we examined the activities of various components of the apoptotic machinery as well as the various signaling

pathways that promote apoptosis. We first examined cytosolic and mitochondrial levels of cytochrome c in the SDHC E69 cells after the establishment and their NIH3T3 progenitors. Cytochrome c is known to be released from mitochondria and combines with apoptosis protease activating factor-1 (Apaf-1), procaspase 9, and dATP in the cytosol, triggering the activation of caspase 3 (*9*). As expected given its role in electron transport, cellular cytochrome c was found in the mitochondria in both the SDHC E69 cells and NIH3T3 cells (Figure 3A). Cytosolic levels in the SDHC E69 cells and NIH3T3 cells were lower than mitochondrial levels. However, cytosolic cytochrome c levels increased significantly in the SDHC E69 cells. This is consistent with the increase in caspase 3 that we have documented previously (*9*) and suggests strongly that elevated O_2^- production in the SDHC E69 cells sets into motion events that enable cytochrome c leakage from mitochondria, with caspase 3 activation and apoptosis the downstream consequences. We then examined the status of two proapoptotic members of the Bcl-2 family. First, we looked at Bax, which regulates cytochrome c release from mitochondria by translocating from the cytoplasm to mitochondria and subsequently altering mitochondrial membrane permeability (*10*). Bax primarily localized to the cytosol. In the mitochondria of the SDHC E69 cells compared to NIH3T3 cells, the Bax levels were significantly higher (Figure 3A). These results suggest that the increased cytosolic cytochrome c levels observed in the SDHC E69 cells could be attributed at least in part to Bax translocation. Second, we analyzed the Bid protein, which is activated by caspase 8 cleavage to produce 15 kDa tBid. tBid translocates to mitochondria to facilitate cytochrome c release by interacting with Bax (*11*). Bid and tBid levels were barely detectable in the SDHC E69 cells (Figure 3A). These results suggest that cytochrome c release was mainly caused by Bax localized in mitochondria. We also examined the activation of the tumor suppressor gene p53, as p53 has long been known to act as a transcription factor to promote apoptosis via Bax action (*12*). More recently, p53 has been also been shown to localize to mitochondria and, in a transcription-independent fashion, play an important role in the mitochondrial apoptotic pathway (*13*). We asked whether p53 might be involved in the cellular responses to the oxidative stress inherent to the SDHC E69 cells. Since p53 levels are normally held low via the action of MDM2, we examined MDM2 mRNA expression using Northern blot analyses. MDM2 mRNA exists in three isoforms: 3.0 kbp, 1.7 kbp and several short-forms (of roughly 1.2 kbp) which are generated by alternative splicing. They are translated into several forms, including p90 (which possesses p53 binding capacity), p76 (which lacks p53 binding ability) and short-form types (which also lack p53 activity and are found in transformed cells) (*14*). In

NIH3T3 cells, MDM2 mRNA expression was equally distributed between the 3.0 kbp and 1.7 kbp mRNAs, which are translated into the p90 and p76 MDM2 proteins, respectively (Figure 3B). A dramatically different pattern was observed in the SDHC E69 cells, as only the short-form type was expressed, which is incapable binding to and promoting p53 protein degradation (Figure 3B). These results led us to test p53 protein levels by Western blot analysis. p53 levels were below the level of detection in NIH3T3 cells (Figure 3C). Conversely, p53 protein existed in copious amounts in the SDHC E69 cells, in which the short-form type MDM2 mRNA was expressed (Figure 3C). Moreover, most of the p53 protein was phosphorylated at serine residue 15 (Figure 3C), a modification known to activate p53 as a transcription factor, leading to cell-cycle arrest and apoptosis (*15*). These results strongly suggest that p53 exists as an active transcription factor in the SDHC E69 cells. We confirmed this in two ways. First, p21 protein, which is a p53 target gene and promotes the cell-cycle arrest, was highly expressed in the SDHC E69 cells but not in NIH3T3 cells (Figure 3C). Second, a luciferase-containing construct with a p53 binding cis-elements was transiently transfected into the each cell lines. Luciferase activity was over 2.8 times higher in the SDHC E69 cells than in the NIH3T3 cells (Figure 3D). Collectively, these data show that in the SDHC E69 cells, the oxidative stress resulting from mitochondrial overproduction of O_2^- leads to altered mRNA expression of MDM2 which in turn results in p53 accumulation and activation. As a consequence, p21 and presumably other p53 target genes are induced, resulting in cell-cycle delays and apoptosis. It is also possible that p53 is present in the mitochondria of the SDHC E69 cells to promote cytochrome c release and trigger apoptosis.

We next analyzed the relative roles played by caspase 8 and caspase 9 in elevated apoptosis in the SDHC E69 cells. Caspase 8 acts as an initiator caspase in the extrinsic apoptotic pathway while caspase 9 is activated by cytochrome c to initiate the intrinsic (mitochondrial) apoptotic pathway (*9*). When cleaved, both proteolytically activate executioner caspases such as caspase 3. We employed caspase 8 and 9 antagonists for this purpose and measured caspase 3 activity. As demonstrated previously, caspase 3 levels were higher in the SDHC E69 cells than in NIH3T3 cells (Figure 4A). In the NIH3T3 cells, caspase 3 activity was slightly decreased by each caspase antagonist ($p < 0.01$) (Figure 4A). Caspase 3 activity was not further reduced by addition of both caspase 8 and 9 antagonists in the NIH3T3 cells (Figure 4A). Since both caspase 8 and 9 participate in the extrinsic pathway, these results suggest that both caspases are active in NIH3T3 cells, albeit at low levels, in response to the low levels of extrinsic oxidative stress normally present in cultured cells. In the SDHC E69 cells, both

caspase 8 and caspase 9 inhibition had a larger effect on caspase 3 activity (Figure 4A). Since caspase 9 acts downstream of mitochondria, this suggests that the elevated apoptosis in the SDHC E69 transformed cells was the result of increased ROS generation in their mitochondria rather than involving the extrinsic pathway, in which case both caspase antagonists would be expected to have roughly equal inhibitory effects. Moreover, we tested the viability of cells cultured in the presence of each caspase antagonist. The survival rate of the NIH3T3 cells was decreased by treatment with a caspase 9 antagonist (Figure 4B). Some necrotic cell death was observed under these conditions (data not shown). Given that necrotic cell deaths were rarely observed in cells not treated with the caspase antagonists, we speculate that one consequence of the caspase 9-induced apoptosis is to protect tissues from stress-induced necrotic cell death that would otherwise result from mitochondrial oxidative stress.

In contrast to the results obtained with NIH3T3 cells, the presence of each caspase antagonist resulted in increased the cell growth and proliferation in the SDHC E69 cells (Figure 4C). This suggests that the SDHC E69 transformed cells might have developed oxidative stress resistance or even dependent cell growth and proliferation mechanisms. Moreover, both caspase 8 and 9 antagonists were inadequate to substantially reduce caspase 3 activity in the SDHC E69 cells ($p <$ 0.01) (Figure 4A). This led us to speculate that a signal transduction pathway might be operative in these cells. Thus, while cytochrome c release from mitochondria was an important intermediary participant, components upstream of the mitochondria and independent of the mitochondria were responsible for initiating the apoptotic process in the SDHC E69 cells.

The Ras-Raf and Ras-MEKK signal transduction pathway has been shown to promote apoptosis in a mitochondria-independent fashion (16). For example, MEKK1 can be cleaved by many stimuli to generate a 91 kDa kinase that is a strong inducer of apoptosis (17,18). We tested to see if some of the elevated apoptosis in the 3-month SDHC E69 cells might be due to the activation of such signal transduction pathways. First, we analyzed p21Ras (H-, N-, K-Ras) and M-Ras mRNA expression levels by Northern blot analysis. Relative to the actin and G3PDH internal controls, p21Ras and M-Ras mRNA expression levels in the SDHC E69 cells were increased in comparison with the NIH3T3 cells (Figure 5A). Second, we tested Raf-1/C-Raf mRNA expression and MEKK1 protein concentration by Northern and Western blot analyses. Relative to the actin and G3PDH internal standards, Raf-1/C-Raf mRNA expression, which induces cell growth and proliferation, was significantly increased in the SDHC E69 cells in comparison to the NIH3T3 cells (Figure 5B). In additional, 195 kDa full-length MEKK1 protein, which can be cleaved to activate caspase 3,

was present in unchanged amount in the SDHC E69 cells, but the activated p91 kDa MEKK1 protein, which induces apoptosis independent of the mitochondrial pathway, was increased (Figure 5C). Thus, it appears that Ras acts to increase MEKK1 expression in response to the oxidative stress and MEKK1 has been cleaved into its active form in the SDHC E69 cells. In addition, we analyzed JNK and p38 MAPK, which are located further downstream in these signal transduction pathways. Activated 54 kDa and 46 kDa JNK proteins were present in increased amounts in the SDHC E69 cells (Figure 5C). Conversely, the accumulation of activated p38 MAPK protein was not altered (Figure 5C). We also performed an AP-1 cis-element-dependent luciferase assay, which serves as a measure of JNK activity. JNK-dependent transcription was activated in the SDHC E69 cells (Figuer 5D).

We speculate that this explains the phenotypes we have previously observed in the SDHC E69 cells; namely, those of increased apoptosis, high levels of transformation into neoplasms and hypermutability. In addition, the growth characteristics of SDHC E69 cells in the epithelium of nude mice appear to mimic the slow growth of PGLs. It has been reported that the hereditary PGLs that are usually characterized by the development of benign, neural-crest-derived, slow-growing tumors of parasympathetic ganglia which are caused by mutations in the SDHC gene. Between 10% and 50% of cases are familial and are transmitted in an autosomal dominant fashion with incomplete and age-dependent penetrance. We speculate that these characteristics are related to the apoptosis induction caused by the mitochondrial.

Acknowledgements

References

1. Turrens JF. Superoxide production by the mitochondrial respiratory chain. Biosci Rep 1997; 17:3-8.
2. Ishii N, Fujii M, Hartman PS, Tsuda M, Yasuda K, Senoo-Matsuda N, Yanase S, Ayusawa D, Suzuki K. A mutation in succinate dehydrogenase cytochrome b causes oxidative stress and aging in nematodes. Nature 1998; 394:694-697.
3. Senoo-Matsuda N, Yasuda K, Tsuda M, Ohkubo T, Yoshimura S, Nakazawa H, Hartman PS, Ishii N. A defect in the cytochrome b large subunit in complex II causes both superoxide anion overproduction and

abnormal energy metabolism in Caenorhabditis elegans. J Biol Chem 2001; 276:41553-41558.

4. Senoo-Matsuda N, Hartman PS, Akatsuka A, Yoshimura S, Ishii N. A complex II defect affects mitochondrial structure, leading to ced-3 and ced-4-dependent apoptosis and aging. J Biol Chem 2003; 278:22031-22036.

5. Hartman PS, Ponder R, Lo HH, Ishii N. Mitochondrial oxidative stress can lead to nuclear mutability. Mech Ageing Develop 2004; 125:417-420.

6. Ishii T, Yasuda K, Akatsuka A, Hino O, Hartman PS, Ishii N. A mutation in the SDHC gene of complex II increases oxidative stress, resulting in apoptosis and tumorigenesis. Cancer Res 2005; 65:203-209.

7. Niemann S, Muller U. Mutations in SDHC cause autosomal dominant paraganmlioma, type 3. Nat Genet 2000; 26:268-270.

8. Baysal BE, Ferrell RE, Willett-Brozick JE, Lawrence EC, Myssiorek D, Bosch A, van der Mey A, Taschner PE, Rubinstein WS, Myers EN, Richard CW 3rd, Cornelisse CJ, Devilee P, Devlin B. Mutations in SDHD, a mitochondrial complex II Gene, in hereditary paraganglioma. Science 2000; 287:848-851.

9. Budihardjo I, Oliver H, Lutter M, Luo X, Wang X. Biochemical pathways of caspase activation during apoptosis. Annu Rev Cell Dev Biol 1999; 15:269-290.

10. Jürgensmeier JM, Xie Z, Deveraux Q, Ellerby L, Bredesen D, Reed JC. Bax directly induces release of cytochrome c from isolated mitochondria. Proc Natl Acad Sci USA 1998; 95:4997-5002.

11. Luo X, Budihardjo I, Zou H, Slaughter C, Wang X. Bid, a Bcl2 interacting protein, mediates cytochrome c release from mitochondria in response to activation of cell surface death receptors. Cell 1998; 94:481-490.

12. Shen Y, White E. p53-dependent apoptosis pathways. Adv Cancer Res 2001; 82:55-84.

13. Mihara M, Erster S, Zaika A, Petrenko O, Chittenden T, Pancoska P, Moll UM. p53 has a direct apoptogenic role at the mitochondria. Mol Cell 2003; 11:577-590.

14. Sigalas I, Calvert AH, Anderson JJ, Neal DE, Lunec J. Alternatively spliced mdm2 transcripts with loss of p53 binding domain sequences: transforming ability and frequent detection in human cancer. Nat Med 1996; 2:912-917.

15. Shieh SY, Ikeda M, Taya Y, Prives C. DNA damage-induced phosphorylation of p53 alleviates inhibition by MDM2. Cell 1997; 91:325-334.

16. Russell M, Lange-Carter CA, Johnson GL. Direct interaction between Ras and the kinase domain of mitogen-activated protein kinase kinase kinase (MEKK1). J Biol Chem 1995; 270:11757-11760.

17. Widmann C, Gerwins P, Johnson NL, Jarpe MB, Johnson GL. MEK kinase 1, a substrate for DEVD-directed caspases, is involved in genotoxin-induced apoptosis. Mol Cell Biol 1998; 18:2416-2429.

18. Gibson EM, Henson ES, Villanueva J, Gibson SB. MEK kinase 1 induces mitochondrial permeability transition leading to apoptosis independent of cytochrome C release. J Biol Chem 2002; 277:10573-10580.

ORIGINAL ARTICLE

A low cost and quick assay system using the free-living nematode *Caenorhabditis elegans* to determine the effects of Kampo medicines on life span

Takuro Yamaguchi[1,2], Akira Onodera[1], Kayo Yasuda[3], Yasunori Nishio[2,4], Makoto Arai[5], Michio Tsuda[1], Masaki Miyazawa[1], Philip S. Hartman[6] and Naoaki Ishii[1,2]

[1] *Department of Molecular Life Science, Tokai University School of Medicine, Japan*
[2] *NemaBio, Inc., Japan*
[3] *Teaching and Research Support Center, Tokai University School of Medicine, Japan*
[4] *Towa Scientific Co., LTD, Japan*
[5] *Department of Oriental Medicine, Tokai University School of Medicine, Japan*
[6] *Biology Department, Texas Christian University, USA.*

Abstract
A low cost and quick assay system has been developed using the free-living nematode *Caenorhabditis elegans* to determine the effects of Kampo medicines (traditional Japanese medicines) on life span. A key characteristic of this system is the use of a *fer-15* mutant, which is sterile when grown at 25°C owing to the production of spermatids that fail to activate into spermatozoa. This prevented the production of progeny, which would otherwise complicate life span analyses. In addition, liquid culture medium permitted easy handling of the test subjects. We employed this system to examine the longevity effects of 26 Kampo medicines and crude drugs. Of these, *Rhei Rhizoma* was found to extend the life span and acts as an anti-oxidant that suppresses superoxide anion generation from mitochondria.

Key words: C. elegans; life span; Kampo medicines; crude drugs; oxidative stress

Introduction
A number of assay systems have been developed to screen chemicals for their ability to confer favorable phenotypes. Most of these systems are *in vitro* or *in vivo* using single-cell organisms or cells in tissue culture, whereas systems using multicellular organism are few owing to both labor and cost intensity. We now report of a low cost and rapid assay system at the whole-animal level that we employed to find natural endowments or chemicals with longevity effects in the free-living nematode *Caenorhabditis elegans* (*C. elegans*). *C. elegans* offers several distinct advantages for aging research at the organismal level (Luo, 2006), not the least of which is a short maximum life span of approximately 30 days (Klass and Hirsh, 1976; Honda *et al.*, 1993)(Fig. 1). Its soma consists of fewer than 1,000 cells including hypodermis, digestive organ, neurons, musculature, and reproductive organs (Sulston and Horvitz, 1977). All of
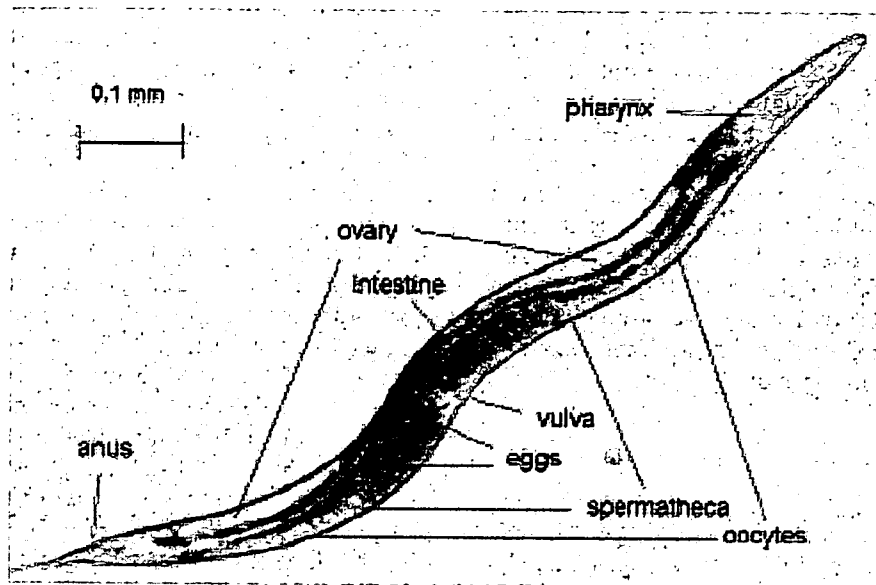
Fig.1 Photomicrograph showing major anatomical features of a *C. elegans* adult hermaphrodite.

these are postmitotic in adults, thus offering the opportunity to detect cumulative age-related cellular alterations (Hosokawa *et al*, 1994; Adachi *et al.*, 1998; Ishii *et al*, 2002). Embryonic development is rapid, taking only 13 h at 20°C (Sulston, 1988; Wood, 1988). After hatching, larval development proceeds through four molts, which punctuate larval stages L1 through L4. Animals reproduce with a rapid life cycle of approximately 3.5 days at 20°C. *C. elegans* also offer an advantage to screen drugs that may increase life span because they live only for 30 days (Melov *et al*, 2000; Ishii *et al*, 2004; Petrascheck *et al*, 2007). In general, *C. elegans* can be readily cultured on agar plate in petri plates on a simple diet of *Escherichia coli* (*E. coli*) (Brenner, 1974). They also can be grown in liquid culture in the presence or absence of bacteria (Vanfleteren, 1980; Jansson *et al*, 1986; Jewitt *at al*, 1999; Houthoofd *et al*, 2002). Liquid culture system is convenient to treat many animals and permitted easy handling of the test subjects rather than agar plate, but animals do not grow well in liquid culture compared to agar plate and seem not to be health because of poor diet. It is known that the life span of *C. elegans* is dependent on the concentration of *E. coli* which often serves as its food (Klass, 1977). In our liquid culture system, Bacto-peptone as nutrition for *E. coli* was increased so that this defect was overcome.

C. elegans normally reproduces as a bisexual hermaphrodite that produces both oocytes and sperm. Animals normally reproduce by self-fertilization. In order to prevent the progeny production, 5-fluoro-2-deoxyuridine (FudR) has generally been used after maturation (Mitchell *et at.*, 1979). In our system, we used *fer-15* mutant, which when grown at 25°C produces spermatids that fail to activate into spermatozoa (Roberts and Ward, 1982). In this report, we introduce a low cost and rapid assay system that examines the life span of a *fer-15* mutant as a marker for the isolation of Kampo medicines and crude drugs with macrobiotic activity.

Kampo medicines (traditional Japanese medicines) and crude drugs are known to have many biological effects. In part owing to the current fitness fad in the world, researchers have attempted to identify chemicals that promote longevity and good health (Kishikawa, *et al.*, 1997). We employed this system to examine 26 Kampo medicines and crude drugs. Of these samples, *Rhei Rhizoma* was found to extend the life span.

Recently, much attention has been focused on the hypothesis that oxidative damage plays a major role in cellular and organismal aging (Finkel and Holbrook, 2000). There are many reports that anti-oxidant agents and enzymes extend life span of several animals, including *C. elegans* (Haenold